Biosensors Hot Paper

Zitierweise:
Internationale Ausgabe: doi.org/10.1002/anie.202007575
Deutsche Ausgabe: doi.org/10.1002/ange.202007575

Transcription Factor Based Small-Molecule Sensing with a Rapid Cell Phone Enabled Fluorescent Bead Assay

*Margaret Chern, Padric M. Garden, R C. Baer, James E. Galagan und Allison M. Dennis**

Abstract: *Recently, allosteric transcription factors (TFs) were identified as a novel class of biorecognition elements for in vitro sensing, whereby an indicator of the differential binding affinity between a TF and its cognate DNA exhibits dose-dependent responsivity to an analyte. Described is a modular bead-based biosensor design that can be applied to such TF-DNA-analyte systems. DNA-functionalized beads enable efficient mixing and spatial separation, while TF-labeled semiconductor quantum dots serve as bright fluorescent indicators of the TF-DNA bound (on bead) and unbound states. The prototype sensor for derivatives of the antibiotic tetracycline exhibits nanomolar sensitivity with visual detection of bead fluorescence. Facile changes to the sensor enable sensor response tuning without necessitating changes to the biomolecular affinities. Assay components self-assemble, and readout by eye or digital camera is possible within 5 minutes of analyte addition, making sensor use facile, rapid, and instrument-free.*

Introduction

Biosensors used in fields as diverse as drug discovery, medicine, food safety, defense, and environmental monitoring depend on recognition moieties such as antibodies for the sensitive and specific detection of molecular analytes.[1,2] Solution phase assays facilitate rapid mixing, while substrate bound assays enable repeated blocking and washing steps. Bead-based assays are an enabling technology that blends the benefits of each of these assay platforms; beads are easily isolated via centrifugation, magnetic separation, or gravimetric settling to facilitate rapid separation and washing steps, while their enhanced surface area enables rapid mixing and high substrate concentrations. The bead assay approach includes antibody-based ELISAs, enzyme-driven reactions, and cell isolation approaches.[3–6]

[*] Dr. M. Chern, Prof. A. M. Dennis
Division of Materials Science and Engineering, Boston University
Boston, MA (USA)
E-Mail: aldennis@bu.edu
P. M. Garden, Prof. J. E. Galagan, Prof. A. M. Dennis
Department of Biomedical Engineering, Boston University
Boston, MA (USA)
Dr. R C. Baer, Prof. J. E. Galagan
Department of Microbiology, Boston University
Boston, MA (USA)
Prof. J. E. Galagan
National Emerging Infectious Diseases Laboratories
Boston University, Boston, MA (USA)
Supporting information and the ORCID identification number(s) for the author(s) of this article can be found under:
https://doi.org/10.1002/anie.202007575.

Antibodies are used as the molecular recognition element in numerous molecular assays, however immunoassay techniques for small molecules are often limited to a competitive format, which have a reduced sensitivity compared to non-competitive approaches,[7,8,10] or require difficult to produce anti-metatype antibodies or other workarounds for noncompetitive detection.[9] Given the challenges of developing immunoassays for small molecules, alternatives such as aptamers and molecularly imprinted polymers have also gained interest, but exhibit their own advantages and disadvantages, particularly with regards to the screening and development effort required to yield effective binders.[11–14] Allosteric TFs are a diverse class of substrate-binding proteins that present a unique opportunity for small-molecule detection because their inherently bifunctional nature provides for both sensing and actuation. In their natural role regulating gene expression,[15] TFs bind or unbind their cognate DNA binding sequence in response to an effector molecule, that is, an analyte. They have been used in synthetic biology as gene expression switches and for detection of small molecules in whole-cell biosensors.[16–19] Only recently have TFs been used for in vitro biosensing,[20,21] including in our recent demonstrations of homogenous and surface-bound Förster resonance energy transfer (FRET) assays.[22–24]

Through this study, we demonstrate a rapid fluorescent bead assay that incorporates semiconductor quantum dots (QDs) and an allosteric transcription factor TF-DNA-analyte system for rapid, small-molecule sensing without the need for subsequent incubation, washing, or signal amplification steps (Figure 1). We selected the prototypical TF-DNA-analyte

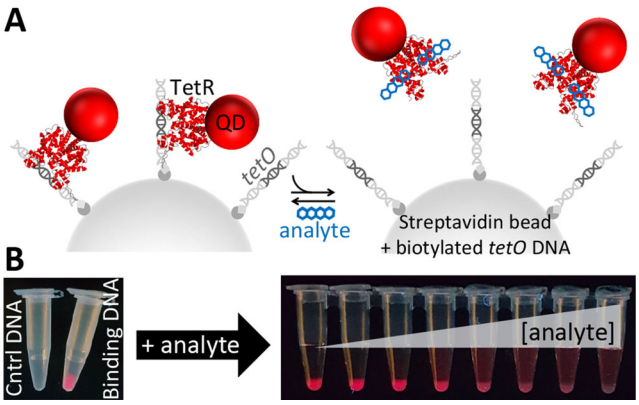

Figure 1. Schematic and general visual of the bead-based pull-down assay. TF-labeled QDs bind streptavidin beads decorated with biotinylated DNA containing the transcription factor (TF) binding sequence (or scrambled control). In the presence of analyte (0–200 nM anhydrotetracycline), the TF unbinds the DNA, redispersing the QDs into the supernatant.

system comprising TetR-*tetO*-anhydrotetracycline (aTc) for this demonstration. TetR responds to the tetracycline family of antibiotics, including the non-antimicrobial variant aTc, which is used as a chemical inducer of protein expression in bacterial systems. TetR dimers bind DNA via a pair of helix-turn-helix domains that tightly bind ($K_D \approx 10^{-11}$ M) to the major grooves of the palindromic *tetO* sequence.[25] When magnesium-chelated aTc binds within the effector (analyte) binding pocket, two amino acids are displaced, causing conformational changes within the protein, shifting the recognition helices and reducing the affinity of TetR for *tetO* by up to nine orders of magnitude.[26] Pairing TetR-*tetO* with a bead platform and fluorescent indicators (i.e., QDs), facilitates macroscopic visualization of this process through spatial separation of the bound and unbound states, resulting in an optical signal transduction mechanism that is both visual and easily quantified. The use of off-the-shelf components and self-assembly-based bioconjugation approaches makes this sensor easy to construct and use, while instrument-free detection enables applications outside the traditional laboratory environment.[27–31]

Results and Discussion

The bead-based biosensor is comprised of four components: 1) commercially available streptavidin-coated agarose beads (SBs), 2) biotinylated DNA containing the TF cognate DNA binding sequence, 3) QDs with a self-assembly-friendly coating for water solubility[32,33] (see Figures S1 and S2 in the Supporting Information), and 4) a histidine-tagged TF. These modular components are mixed together for sensor construction using affinity-based self-assembly (Figures S3 and S4). Mixing commercially available SBs ($\approx$50–100 μm in diameter) with biotinylated double-stranded DNA oligomers produces the solid support for the assay. The relatively large bead size ensures separation of the bead and solution through simple sedimentation in <5 minutes. In our prototype, histidine-tagged TetR self-assembles to the surface of red-emitting QDs due to the affinity of histidine for the zinc on the QD surface.[32–35] When mixed, the TetR-labeled QDs bind beads decorated with the TetR cognate *tetO* DNA sequence. In control reactions using a scrambled DNA oligo, TetR-QD complexes do not bind (Figure 1). Addition of the analyte, aTc, releases the TetR-QD complex from the bead. The bead pellet becomes visibly less fluorescent, while the supernatant exhibits a discernable red photoluminescence (PL). This analyte response is dose-dependent, generating a clear change in signal in just a couple of minutes without the need for additional separation or washing (Figure 1).

Prior to assessing analyte responsivity, we studied the impact of the number of TFs per QD on the sensor assembly. SB slurry was mixed with biotinylated *tetO* oligos and washed, while QDs were independently incubated with varying concentrations of histidine-tagged TetR. When the beads and QDs were mixed, the solutions comprised $\approx$2 μM DNA and 50 nM QDs, leading to a 40:1:*n* ratio of *tetO*:QD:TetR, where $n = 1$, 2, 4, or 8 TetR monomers. By comparing the UV/Vis absorbance of the TetR-labeled QDs to the absorbance of the same solution after the addition of SB:*tetO*, we calculate the fraction of QDs bound to the SB:*tetO* beads and removed from solution by gravimetric settling (Figure 2). As the TetR

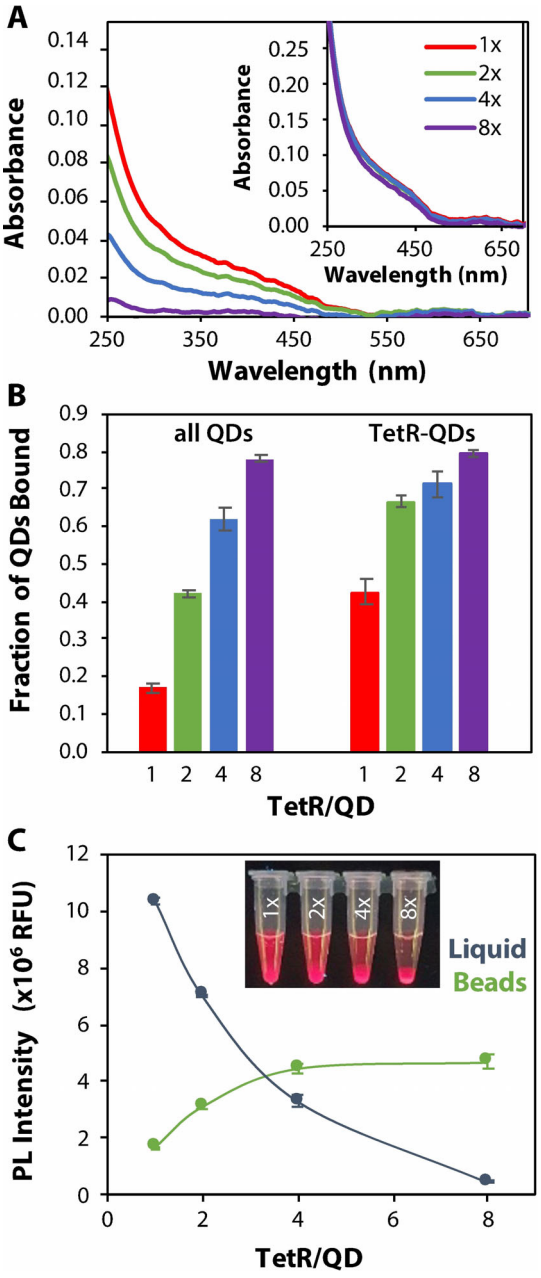

Figure 2. Effect of TetR/QD ratio on QD-Bead loading. A) The absorbance of TetR-labeled QDs before (inset) and after QDs are removed from solution by binding and pelleting with the *tetO*-labeled beads. The numbering indicates the number of TetR monomers per QD. B) The fraction of the QDs bound to the beads (left) increases with TetR labeling density (i.e., the average number of TetR monomers per QD). Normalizing to the number of TetR-labeled QDs using a Poisson distribution of dimerized TetR loading eliminates the impact of QDs without TetR on their surface, demonstrating the fraction of TetR-conjugated QDs bound to the beads (right). C) Photoluminescence intensity of the beads and supernatant confirm the difference in QD loading between the different TetR/QD ratios. The decrease in supernatant PL between the 4× and 8× samples demonstrates increased binding, indicating that the plateau in fluorescence of the bead pellet between the two samples is a result of inner filter effects or QD self-quenching.

loading ratio increases, QD binding to the SB:*tetO* also increases. This increase in QD binding is in part related to the more comprehensive labeling of QDs in the solution: polyhistidine self-assembly on a QD surface results in a mixed population of QDs with the range of protein numbers on the nanoparticle surface following a Poisson distribution.[34] The TetR dimer is known to be very strongly preferred over the monomeric form of the protein,[36] and the his-tag binding of protein subunits to a QD surface has been shown to further stabilize multimeric proteins.[37] Thus, assuming complete dimerization, 40%, 63%, 87% and 98% of QDs are functionalized with at least one TetR dimer at the 1, 2, 4, and 8× loading densities, respectively. With the contribution of unlabeled QDs accounted for, the fraction of TetR dimer-labeled QDs bound to the SBs increases with higher TetR loading concentrations (Figure 2B), but the effect is less pronounced, indicating that some but not all of the stoichiometry-based impact is a result of reducing the number of unlabeled QDs in the solution.

Photoluminescence of the bead pellet and supernatant also indicate increased QD binding to the SB:*tetO* with higher TetR loading (Figure 2C). The supernatant PL peak intensity decreases as the number of TetRs per QD is increased, confirming that the number of unbound QDs is minimized by increasing the TetR concentration. Interestingly, although the percentage of QDs bound to the beads continues to increase as TetR/QD increases, the bead brightness does not increase from the 4× to 8× case, which could be due to inner filter effects or QD self-quenching.[32,38] Buffer exchanging the 1, 2, and 4× TetR/QD bead assemblies before use removes excess QDs (Figure S4), a step that is not required for the 8× system. Notably, varying the QD concentration while maintaining 8× TetR/QD reduces the QD self-quenching at low concentrations and fully saturates the beads leading to unbound QDs at high concentrations (Figure S5).

Sensor response is easily discerned by eye, enabling a qualitative instrument-free sensor output (Figure 3A). Large batches of bead sensors were assembled at all four of the TetR/QD loading ratios with 50% (v/v) SB slurry (Millipore Sigma S1638), 0.2 nmol bt-DNA/50 µL SB, 50 nM QD, and 50, 100, 200, or 400 nM TetR for the 1, 2, 4, and 8× TF/QD sensors, respectively. After assembly, excess QDs were removed with buffer exchange (Figure S3). The beads were aliquoted into a series of 0.2 mL PCR tubes and diluted by half with 2× titrated solutions of aTc; thus, the final assays comprised 25% (v/v) SB, 0.1 nmol bt-DNA, 25 nM QD, and 0–200 nM aTc in 100 µL. After flicking the tubes briefly to mix the buffer and slurry, the tubes were placed on the benchtop for several minutes to allow the bead slurry to settle.

Visual examination of the tubes under UV illumination, documented through digital images, shows that either bead or supernatant brightness can be used to determine general aTc concentrations, with the visual limit of detection (vLOD) varying depending on the TetR/QD ratio. For the 1× TetR/QD ratio, differences in the supernatant brightness are not discernable by eye, but the change in bead fluorescence is visibly distinguishable between 25 and 100 nM aTc. For the 2, 4, and 8× TetR/QD ratios, the change in bead brightness is visible but more subtle. In contrast, the released QDs are easily discerned in the supernatant. The vLOD for the sensor increases from 12.5 nM to 25 nM to 50 nM as the TetR/QD ratio increases from 2 to 4 to 8, respectively, based on the onset of visible red emission in the supernatant. The increase in TetR in the sensor system requires more analyte binding to completely neutralize the DNA binding capacity of any given QD. This TF concentration-dependent effect indicates that the sensitivity of the assay can be tuned to a desired cutoff concentration through device configuration without requiring modification to the biomolecular components used for analyte recognition. This ability to tune the sensor sensitivity by adjusting the protein conjugation density nicely complements

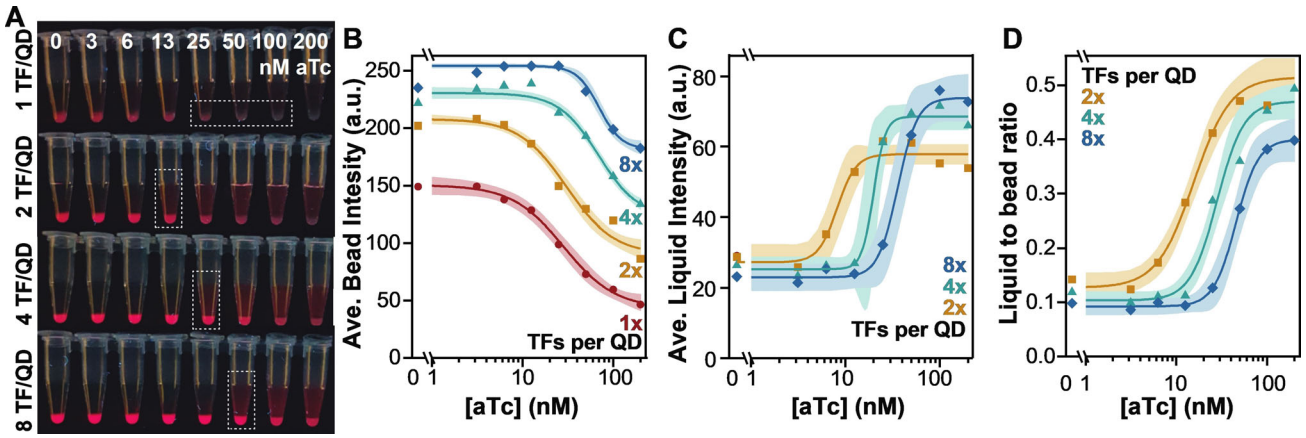

Figure 3. Single-color sensor dose response. A) Sensor visual limit of detection (vLOD) tuned by varying TF/QD ratio. Images of QD:TF + DNA:SB with titration of small-molecule analyte anhydrotetracycline (aTc). vLOD determined by examining bead (1× TF/QD) or supernatant (2, 4, and 8× TF/QD) brightness. Boxes indicate the lowest concentrations with visual discrimination between the adjacent tubes, i.e., the vLOD. B & C) The average red channel pixel intensities from the middle 50 percent of the pixels in the (B) bead and (C) liquid regions of the images in (A) plotted vs. aTc concentration. (D) Dose-dependent red channel liquid-to-bead intensity ratios. Outliers due to light scattering off lint or the side of the tube were eliminated by thresholding on the blue channel (see SI). Shaded regions on plots represent the 95% confidence intervals of fits to the Hill equation weighted with the standard deviations of the pixel intensity averages.

sensitivity tuning based on modifying the DNA[22] or TF[23] to vary binding affinities, which we have demonstrated in our previous FRET-based assays. In any of these systems, combining sensors of various sensitivity into a single assay has the potential to extend the sensor detection range.

While qualitative sensing may be performed using the vLOD, image analysis enables quantitative sensing using the bead assay and a simple digital camera. In addition to the low-cost and ubiquity of digital cameras, image-based analysis is compelling because the spatial separation achieved through simple gravimetric settling of the beads obviates the need for any physical separation of the bound and unbound sensor components or washing steps. Analysis of the assay images shows the dose-dependent decrease in bead fluorescence and concomitant increase in supernatant fluorescence (Figure 3B,C), with comparison to fluorimeter-based measurements confirming the trend (Figure S6). The spatial separation of the bound and unbound QDs enables a ratiometric output of the liquid and bead emission intensities (Figure 3D).

To generate differences in hue, we also designed a two-color, ratiometric sensor using irreversibly bound, green-emitting biotinylated QDs in conjunction with the analyte-responsive red emitters. Adding more green beads to a fixed number of red beads changes the dominance of one color over the other and the perceived color of the bead pellet before analyte addition. As with the single-color sensor, the concentration at which one sees a distinct change in color can be tuned through device design (Figure 4), which is a convenient addition to the biomolecular affinity-based analyte responsivity tuning we have demonstrated in our previous work.[22,23] The red and green emission are completely separated into the red and green channels of the RGB digital image (Figure S7), facilitating quantitative assessment of the red/green emission ratio in the bead pellet. The two-color bead assay enables ratiometric analysis based on the ratio of the green and red channel intensities in the bead pellet (Figure 4E) as well as on the red channel intensity in the liquid and bead regions (Figure 4F).

We also demonstrated sensor compatibility with fetal bovine serum (FBS), a critical preliminary step in exploring the efficacy of this assay in complex biofluids. (Figure S8A–C). The linearity of the assay response in a media dilution series indicates that the assay performs as expected within this concentration range of spiked serum samples. Finally, we successfully demonstrated the detection of doxycycline, a tetracycline-class antibiotic and antiparasitic in clinical use, in complex media. (Figure S8D–F). The cross-reactivity of TetR for a number of tetracyline derivates means that this system can likely be easily adapted to detect tetracycline, chlortetracycline, and oxytetracycline, which are frequently used in agriculture and monitored in foodstuffs and wastewater.[39,40]

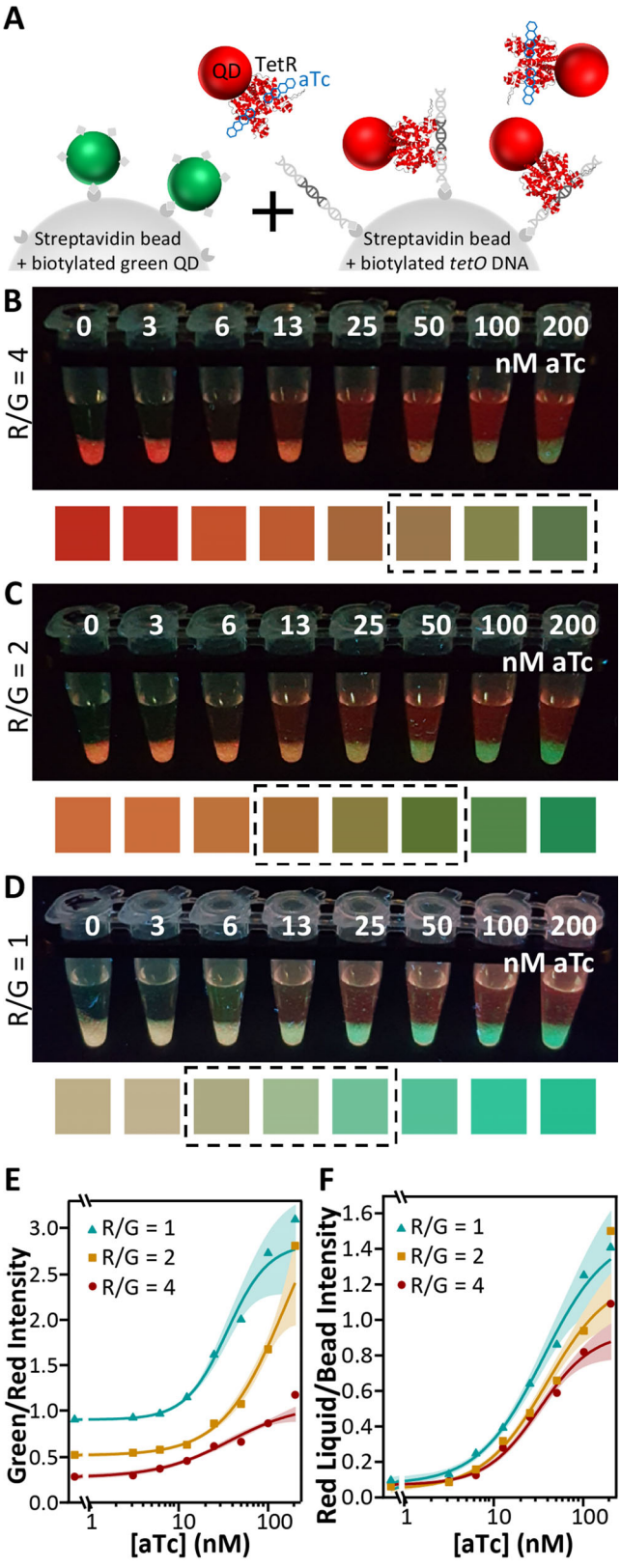

Figure 4. Two-color bead assay. A) To create a ratiometric sensor, beads exhibiting reversible labeling with red QDs via TF-DNA binding are mixed with beads irreversibly labeled with green, biotinylated QDs. In the presence of analyte, only the red QDs unbind; the change in the ratio of red and green QDs in the bead pellet produces a visible color change. B–D) Titration of aTc to sensors with varying ratios of red and green beads produces color changes that are easily discerned by eye. Color maps of the bead photoluminescence show that the concentration range exhibiting the most pronounced color change shifts with the red/green ratio without any change in the sensor biochemistry.

In applications where only one tetracycline derivative is likely to be present (e.g., pharmacokinetic assessments following dosing with a single, known antibiotic), cross-reactivity within the tetracycline family should not be problematic. However, if greater analyte specificity is desired in future applications, mutagenesis and directed evolution of TFs yields substantial improvements in both the specificity and sensitivity of binding.[41]

This demonstration of a rapid, visual sensor for small-molecule detection using an allosteric TF as the primary sensing molecule further demonstrates the potential for TFs in cell-free in vitro sensing applications. The capacity for TF sensing is not constrained to known TF-DNA-analyte triads. Analysis of 145 prokaryotic genomes by Ulrich et al. found at least 17000 one-component signaling proteins.[43] These proteins contain both a sensory and regulatory domain allowing them to sense small molecules, proteins, or other environmental signals and subsequently regulate cell activity. 84% of these proteins contained helix-turn-helix domains, indicating direct DNA binding activity.[42] Even if only a small portion of these are unique allosteric TFs, this study indicates that there are numerous potential sensing proteins to explore. Moreover, for targeted identification of TFs for specific analytes, TFs can be identified through genomic and experimental screens,[22,43] mutated or evolved to change ligand specificity or sensitivity,[41,44,45] or engineered from known binding domains.[46–48] This combination of native and engineered specificity yields countless TF-based sensing opportunities.

Conclusion

In summary, we have developed a rapid, antibody-free, bead-based assay that facilitates the rapid detection of a prototypical small-molecule analyte with a visual readout based on TF-DNA binding. Preparation of the device with multiple TFs per QD ensured high initial binding, eliminating the need for any wash steps in the sensor assembly or assay execution. The combination of color (RGB) and spatial information (bead vs. liquid) provides options for multiple assay readouts such as the red emission intensity from the bead, liquid, or their ratio as well as bead green to red emission intensity ratios. The sensor is easy to assemble, simple to use, and provides results less than 5 minutes after addition of the analyte without washing steps or the assistance of any laboratory equipment. Initial results are promising for the application of this sensor design to detecting the presence of pharmaceuticals such as antibiotics in complex media like serum. The sensor's facile construction and modularity paired with its fast, simple, and instrument-free read-out makes it the perfect template for further development towards rapid detection of small-molecule analytes in the lab, field, and point-of-care settings.

Acknowledgements

The authors acknowledge the helpful discussions and material support afforded by their larger collaborative effort, which includes Mingfu Chen and Dr. Chloé Grazon from the lab of Prof. Mark Grinstaff, Dr. Andy Fan, Prof. Mario Cabodi, and the lab of Prof. Catherine Klapperich. The authors thank Dr. Chloé Grazon and Thuy T. Nguyen for lending materials that allowed for the experimentation that led to proof of concept for this project as well as Wenhan Cao and Prof. Keith Brown for providing training and access to their fluorescence microscope. We also thank the Biointerface Technologies (BIT) core facilities in the Boston University Department of Biomedical Engineering for access to their plate reader. Financial support provided to R.C.B., J.E.G., and A.M.D. through DARPA grant W911NF-16-C-0044. A.M.D. and P.M.G. acknowledge support from the National Institutes of Health National Institute of General Medical Sciences through Grant Number R01GM129437. This work was performed in part at the Center for Nanoscale Systems (CNS), a member of the National Nanotechnology Coordinated Infrastructure Network (NNCI), which is supported by the National Science Foundation under NSF award no. 1541959. CNS is part of Harvard University. The research team includes members of the Boston University Precision Diagnostics Center, Nanotechnology Innovation Center (BUnano), Photonics Center, Cancer Center, and Neurophotonics Center.

Conflict of interest

The authors note a pending patent covering this work (PCT/US2018/063852).

Stichwörter: biosensors · DNA · fluorescence · quantum dots · transcription factors

[1] A. P. F. Turner, *Chem. Soc. Rev.* **2013**, *42*, 3184–3196.
[2] S. Vigneshvar, C. C. Sudhakumari, B. Senthilkumaran, H. Prakash, *Front. Bioeng. Biotechnol.* **2016**, *4*, 11.
[3] X. H. Gao, W. C. W. Chan, S. M. Nie, *J. Biomed. Opt.* **2002**, *7*, 532–537.
[4] C. T. Lim, Y. Zhang, *Biosens. Bioelectron.* **2007**, *22*, 1197–1204.
[5] H. C. Tekin, M. A. M. Gijs, *Lab Chip* **2013**, *13*, 4711–4739.
[6] M. F. Elshal, J. P. McCoy, *Methods* **2006**, *38*, 317–323.
[7] T. M. Jackson, R. P. Ekins, *J. Immunol. Methods* **1986**, *87*, 13–20.
[8] R. Wilson, *Expert Rev. Proteomics* **2013**, *10*, 135–149.
[9] A. González-Techera, H. J. Kim, S. J. Gee, J. A. Last, B. D. Hammock, G. González-Sapienza, *Anal. Chem.* **2007**, *79*, 9191–9196.
[10] X. Wang, L. Cohen, J. Wang, D. R. Walt, *J. Am. Chem. Soc.* **2018**, *140*, 18132–18139.
[11] M. McKeague, M. C. Derosa, *J. Nucleic Acids* **2012**, *2012*, 748913.
[12] W. Zhou, P.-J. Jimmy Huang, J. Ding, J. Liu, *Analyst* **2014**, *139*, 2627–2640.
[13] J. J. BelBruno, *Chem. Rev.* **2019**, *119*, 94–119.
[14] L. I. Andersson, *J. Chromatogr. B* **2000**, *739*, 163–173.
[15] L. Cuthbertson, J. R. Nodwell, *Microbiol. Mol. Biol. Rev.* **2013**, *77*, 440–475.
[16] R. Mahr, J. Frunzke, *Appl. Microbiol. Biotechnol.* **2016**, *100*, 79–90.
[17] S. Raman, J. K. Rogers, N. D. Taylor, G. M. Church, *Proc. Natl. Acad. Sci. USA* **2014**, *111*, 17803–17808.
[18] M. Park, S. L. Tsai, W. Chen, *Sensors* **2013**, *13*, 5777–5795.

[19] R. Fernandez-Lopez, R. Ruiz, F. de la Cruz, G. Moncalian, *Front. Microbiol.* **2015**, *6*, 648.
[20] S. S. Li, L. Zhou, Y. P. Yao, K. Q. Fan, Z. L. Li, L. X. Zhang, W. S. Wang, K. Q. Yang, *Chem. Commun.* **2017**, *53*, 99 – 102.
[21] J. Cao, Y. Yao, K. Fan, G. Tan, W. Xiang, X. Xia, S. Li, W. Wang, L. Zhang, *Sci. Adv.* **2018**, *4*, eaau4602.
[22] C. Grazon, R C. Baer, U. Kuzmanović, T. Nguyen, M. Chen, M. Zamani, M. Chern, P. Aquino, X. Zhang, S. Lecommandoux, A. Fan, M. Cabodi, C. Klapperich, M. W. Grinstaff, A. M. Dennis, J. E. Galagan, *Nat. Commun.* **2020**, *11*, 1276.
[23] T. T. Nguyen, M. Chern, R C. Baer, J. Galagan, A. M. Dennis, *Small* **2020**, *16*, 1907522.
[24] M. Chen, T. T. Nguyen, N. Varongchayakul, C. Grazon, M. Chern, R C. Baer, S. Lecommandoux, C. M. Klapperich, J. E. Galagan, A. M. Dennis, M. W. Grinstaff, *Adv. Healthcare Mater.* **2020**, *9*, 2000403.
[25] O. Scholz, P. Schubert, M. Kintrup, W. Hillen, *Biochemistry* **2000**, *39*, 10914 – 10920.
[26] P. Orth, W. Saenger, W. Hinrichs, *Biochemistry* **1999**, *38*, 191 – 198.
[27] E. Petryayeva, W. R. Algar, *RSC Adv.* **2015**, *5*, 22256 – 22282.
[28] E. Petryayeva, W. R. Algar, *Anal. Chem.* **2014**, *86*, 3195 – 3202.
[29] E. Petryayeva, W. R. Algar, *Analyst* **2015**, *140*, 4037 – 4045.
[30] H. Zhu, U. Sikora, A. Ozcan, *Analyst* **2012**, *137*, 2541 – 2544.
[31] M. Chern, J. C. Kays, S. Bhuckory, A. M. Dennis, *Methods Appl. Fluoresc.* **2019**, *7*, 36.
[32] M. Chern, T. T. Nguyen, A. H. Mahler, A. M. Dennis, *Nanoscale* **2017**, *9*, 16446 – 16458.
[33] K. Susumu, E. Oh, J. B. Delehanty, J. B. Blanco-Canosa, B. J. Johnson, V. Jain, W. J. Hervey, W. R. Algar, K. Boeneman, P. E. Dawson, I. L. Medintz, *J. Am. Chem. Soc.* **2011**, *133*, 9480 – 9496.
[34] T. Pons, I. L. Medintz, X. Wang, D. S. English, H. Mattoussi, *J. Am. Chem. Soc.* **2006**, *128*, 15324 – 15331.
[35] A. M. Dennis, D. C. Sotto, B. C. Mei, I. L. Medintz, H. Mattoussi, G. Bao, *Bioconjugate Chem.* **2010**, *21*, 1160 – 1170.
[36] H. Backes, C. Berens, V. Helbl, S. Walter, F. X. Schmid, W. Hillen, *Biochemistry* **1997**, *36*, 5311 – 5322.
[37] J. N. Vranish, M. G. Ancona, E. Oh, K. Susumu, G. Lasarte Aragonés, J. C. Breger, S. A. Walper, I. L. Medintz, *ACS Nano* **2018**, *12*, 7911 – 7926.
[38] J. R. Lakowicz, *Principles of Fluorescence Spectroscopy*, 3rd ed., Springer, New York, **2006**, p. xxvi, p. 954.
[39] F. Granados-Chinchilla, C. Rodríguez, *J. Anal. Methods Chem.* **2017**, *2017*, 1315497.
[40] R. Daghrir, P. Drogui, *Environ. Chem. Lett.* **2013**, *11*, 209 – 227.
[41] A. J. Meyer, T. H. Segall-Shapiro, E. Glassey, J. Zhang, C. A. Voigt, *Nat. Chem. Biol.* **2019**, *15*, 196 – 204.
[42] L. E. Ulrich, E. V. Koonin, I. B. Zhulin, *Trends Microbiol.* **2005**, *13*, 52 – 56.
[43] B. C. Stanton, A. A. K. Nielsen, A. Tamsir, K. Clancy, T. Peterson, C. A. Voigt, *Nat. Chem. Biol.* **2014**, *10*, 99 – 105.
[44] S.-Y. Tang, P. C. Cirino, *Angew. Chem. Int. Ed.* **2011**, *50*, 1084 – 1086; *Angew. Chem.* **2011**, *123*, 1116 – 1118.
[45] F. M. L. Machado, A. Currin, N. Dixon, *J. Biol. Eng.* **2019**, *13*, 91.
[46] N. D. Taylor, A. S. Garruss, R. Moretti, S. Chan, M. A. Arbing, D. Cascio, J. K. Rogers, F. J. Isaacs, S. Kosuri, D. Baker, S. Fields, G. M. Church, S. Raman, *Nat. Methods* **2016**, *13*, 177 – 183.
[47] J. F. Juárez, B. Lecube-Azpeitia, S. L. Brown, C. D. Johnston, G. M. Church, *Nat. Commun.* **2018**, *9*, 3101.
[48] S. Raman, N. Taylor, N. Genuth, S. Fields, G. M. Church, *Trends Genet.* **2014**, *30*, 521 – 528.

Manuskript erhalten: 26. Mai 2020
Endgültige Fassung online: ■■. ■■ ■■■■

Forschungsartikel

Biosensors

M. Chern, P. M. Garden, R C. Baer, J. E. Galagan, A. M. Dennis* _____ ▮▮▮▮–▮▮▮▮

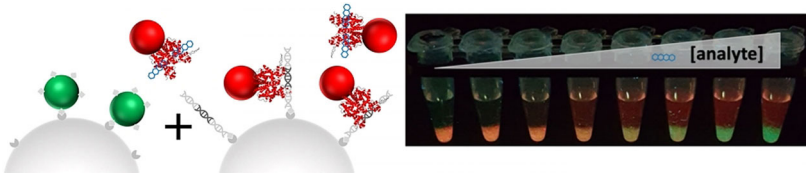

Transcription Factor Based Small-Molecule Sensing with a Rapid Cell Phone Enabled Fluorescent Bead Assay

The allosteric transcription factor TetR acts as a sensor and actuator in this quantum dot enabled fluorescent bead assay for the small molecule anhydrotetracycline. This rapid, antibody-free biosensor produces a visible change in fluorescent color, which can be detected either by eye or by using an inexpensive digital camera, based on dose-dependent analyte-responsive protein-DNA binding. The adaptable sensor uses easily accessible biomolecular components.